


Long-Range Retarded Elastic Metamaterials: Wave-Stopping, Negative, and Hypersonic or Superluminal Group Velocity

A. Carcaterra,^{*} F. Coppo, F. Mezzani, and S. Pensalfini

Department of Mechanical and Aerospace Engineering, Sapienza University, Rome 00184, Italy

 (Received 19 February 2018; revised manuscript received 28 November 2018; published 22 January 2019)

We investigate new phenomena in elastic wave propagation in metamaterials characterized by long-range interactions. The kind of waves in this context reveal wave-stopping, negative group velocity, instability, and hypersonic or superluminal effects both for instantaneous and for nonlocal retarded actions. Closed-form results are presented and a universal propagation map synthesizes the expected properties of these materials. Perspectives in physics, engineering, and social dynamics are discussed.

DOI: [10.1103/PhysRevApplied.11.014041](https://doi.org/10.1103/PhysRevApplied.11.014041)

I. INTRODUCTION

Metamaterials are known to yield unexpected results in many applications. For example, in electromagnetics these are frequently related to an anomalous refraction index and dissipation. Studies have demonstrated unusual wave propagation [1] by creating negative group velocity (NGV), or light-stopping [2–5], or fast light using special dissipation and diffraction properties of electromagnetic media [6–9]. Even an acoustic setup was proposed in Ref. [10], where, with electronically assisted devices, wave trains of desired spectral composition and superluminal wave propagation were observed [11]. Waves in plasmas and charged gases are also a stimulating example of acoustic fields controlled by long-range electrical interactions [12–15]. In mechanics, metamaterials introduced micropolar, higher-gradient, and nonlocal elasticity [16–24].

In one of the rare investigations of nonlocal dispersion relationship, Eringen [20] identifies the long-range elastic modulus, based on Brillouin dispersion in a lattice [25], which he compares successfully with experimental results [26]. Even in the landscape of recent investigations of elastic metamaterials, the correlation between waves and nonlocality is not directly addressed [27] and the scientific literature does not report results on anomalous elastic wave propagation analogous to those found in electromagnetics. Even though nonlocal interactions have been investigated in several areas [20, 28–32], the lack of general results for dispersive properties in nonlocal materials should not be surprising since theoretical investigations in this field suggest complex integral-differential equations in space and differential equations in time to describe the wave propagation. In the present paper, the dispersion relationship is analytically determined for

elastic materials with long-range and retarded constitutive relationships, yielding surprising wave-propagation behaviors—namely, wave-stopping and negative and hypersonic or superluminal group velocity—as a direct effect of nonlocality.

Dissipation effects are also included in the model, but it is shown they do not represent a necessary condition to produce superluminal propagation. The derivations presented here allow discussion in detail of the wave-propagation scenarios related to the elastic long-range interactions, unveiling the unexpected effects previously mentioned. The approach used here considers long-range interactions by examining their connectivity characteristics. Unlike in classical waves, which are borne out of particle-particle connections between the closest neighbors, unconventional effects result when one-to-all-particles connections are introduced, as in Refs. [33–38], and when all-to-all connections appear, as in Vlasov's theory [39] or in quantum physics [40,41], or in the case of elastic materials investigated here.

The mechanism for wave-stopping, negative group velocity, and hypersonic (superluminal) propagation illustrated in this paper is demonstrated by simple long-range forces. The particle-particle interaction forces in this case rapidly decay with the distance and asymptotically vanish, as in many physical forces; namely, electrostatic, magnetostatic, and gravitational forces. These interaction forces are represented in this paper by two families of exponentially decaying functions, the Gauss-like and Laplace-like functions, which lead to expressions for dispersion relationships. Three regimes of interactions are demonstrated, according to the distance range and the intensity of the force, quantified by the long-range elastic modulus E^* : (i) negative group velocity and wave-stopping, (ii) hypersonic (superluminal) group velocity and instability, and (iii) eigenstate migration.

^{*}antonio.carcattera@uniroma1.it

The existence of hypersonic or superluminal waves stimulated additional investigation of the retarded long-range actions. It is shown that, even when a particle-particle interaction is retarded because of its finite speed v_f , the group velocity can still be hypersonic (superluminal), even with negative group velocity, and the phase speed can overcome the upper bound v_f as well.

These effects were investigated in authoritative studies by Brillouin, Sommerfeld, and Voigt (see Ref. [42]) that show they fit the framework of relativity, since group and phase velocities do not coincide with the signal velocity, which indeed is always confined below the upper bound of the speed of light.

The terms ‘‘hypersonic’’ and ‘‘superluminal’’ are used in this paper for sound and light, respectively to indicate very fast waves that can exceed the phase or group velocity of sound or light, respectively, depending on the nature of the D’Alembert waveguide and on the value of v_f .

II. EQUATION OF MOTION

In this section, we analyze the case of long-range force, additionally with respect to the classical elastic interaction. We define $\mathbf{F}(\mathbf{P}, \mathbf{Q})$ as the force acting on the particle at \mathbf{P} because of the particle at \mathbf{Q} (Fig. 1). \mathbf{F} should guarantee the action-reaction principle holds:

$$\mathbf{F}(\mathbf{P}, \mathbf{Q}) = -\mathbf{F}(\mathbf{Q}, \mathbf{P}). \quad (1)$$

The force between two material elements in the initial reference configuration at \mathbf{x} and $\boldsymbol{\xi}$, respectively, can be

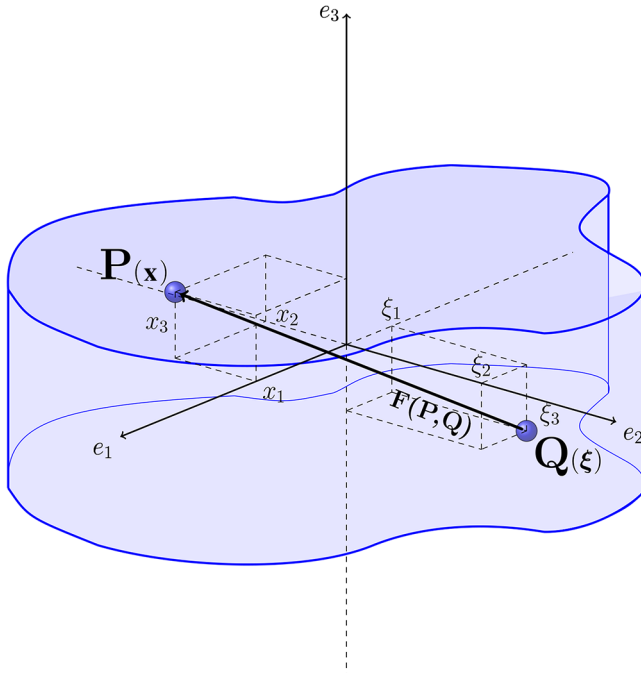


FIG. 1. Long-range interaction.

expressed as

$$\mathbf{F}[\mathbf{x} + \mathbf{u}(\mathbf{x}, t), \boldsymbol{\xi} + \mathbf{u}(\boldsymbol{\xi}, t)] = -f(|\mathbf{r}|)\mathbf{r}, \quad (2)$$

where

$$\mathbf{r} = \mathbf{x} - \boldsymbol{\xi} + \mathbf{u}(\mathbf{x}, t) - \mathbf{u}(\boldsymbol{\xi}, t), \quad (3)$$

where $\mathbf{u}(\mathbf{x}, t)$ is the displacement in the elastic medium, and with the convention introduced by Eq. (2) it follows that $f(|\mathbf{r}|)$ is negative for repulsive force and positive for attractive force.

Forces decaying with $|\mathbf{r}|$, such that $\lim_{|\mathbf{r}| \rightarrow \infty} f(|\mathbf{r}|)\mathbf{r} = 0$, are considered here. This property is typical, for example, of magnetostatic, Coulomb, and gravitational forces.

The nature of long-range interactions leads to nonlinear integral-differential equations to describe the wave propagation. Starting from the Navier-Cauchy formulation, we obtain for a continuous unbounded three-dimensional elastic solid

$$\rho \mathbf{u}_{,tt}(\mathbf{x}, t) - \frac{E}{2(1+\nu)} \left\{ \nabla^2 \mathbf{u}(\mathbf{x}, t) + \frac{1}{1-2\nu} \nabla [\nabla \cdot \mathbf{u}(\mathbf{x}, t)] \right\} + \int_{\boldsymbol{\xi} \in \mathbb{R}^3} f(|\mathbf{r}|)\mathbf{r} dV = 0, \quad (4)$$

where the subscript t indicates derivation with respect to time, ρ , E , and ν the density, the Young’s modulus, and the Poisson ratio of the medium, respectively, and ∇ is the Laplace operator.

The integral represents the sum of nonconventional long-range forces and is the focus of this paper.

For acoustic media with long-range interactions (the case of electrostatic approximation of a low-frequency plasma [43]) the equation of motion can be simplified as $\square u(\mathbf{x}, t) + \int_{\boldsymbol{\xi} \in \mathbb{R}^3} f(|\mathbf{r}|)\mathbf{r} dV = 0$, where \square stands for the D’Alembert operator. In general, analytical solutions are not possible. However, the linearization of the force $f(|\mathbf{r}|)$ with respect to $\boldsymbol{\varepsilon} = \mathbf{u}(\mathbf{x}, t) - \mathbf{u}(\boldsymbol{\xi}, t)$ and for small deformation permits, together with some additional hypotheses introduced later, the investigation of closed-form solutions, providing important insights into the wave-propagation properties.

The Taylor series of the force up to the first order in terms of $\boldsymbol{\varepsilon}$ is

$$f(|\mathbf{r}|)\mathbf{r} \sim (\mathbf{x} - \boldsymbol{\xi})f_0 + \mathbf{h}_0\boldsymbol{\varepsilon} + f_0\boldsymbol{\varepsilon}, \quad (5)$$

where

$$f_0 = f(|\mathbf{x} - \boldsymbol{\xi}|), \quad (6)$$

$$\mathbf{h}_0 = \left. \frac{\partial f}{\partial |\mathbf{r}|} \right|_0, \frac{(\mathbf{x} - \boldsymbol{\xi}) \otimes (\mathbf{x} - \boldsymbol{\xi})}{|\mathbf{x} - \boldsymbol{\xi}|} \quad (7)$$

and the subscript 0 denotes quantities evaluated at $\boldsymbol{\varepsilon} = \mathbf{0}$. Here \otimes is the tensor-product operator.

Therefore, the linearized integral term of equation of motion (4) becomes

$$\int_{\xi \in \mathbb{R}^3} [(\mathbf{x} - \xi)f_0 + \mathbf{h}_0 \boldsymbol{\varepsilon} + f_0 \boldsymbol{\varepsilon}] dV. \quad (8)$$

Separation of the static and dynamic components of the displacement, $\mathbf{u}(\mathbf{x}, t) = \mathbf{v}(\mathbf{x}) + \mathbf{w}(\mathbf{x}, t)$, leads to

$$\begin{aligned} \rho \mathbf{w}_{tt} + \frac{E}{2(1+\nu)} \left[\nabla^2 \mathbf{w} - \frac{1}{1-2\nu} \nabla (\nabla \cdot \mathbf{w}) \right] + \bar{\mathbf{h}}_0 \cdot \mathbf{w} \\ - [\mathbf{h}_0 * \mathbf{w}] + \bar{f}_0 \mathbf{w} - [f_0 * \mathbf{w}] = 0, \end{aligned} \quad (9)$$

for the dynamic component, where the bar indicates average over \mathbb{R}^3 and the asterisk indicates the convolution operator.

In this wave-dynamics context, we are not interested in the discussion of $\mathbf{v}(\mathbf{x})$. Indeed, for those forces that obey

$$\int_{\xi \in \mathbb{R}^3} (\mathbf{x} - \xi) f_0 dV = 0, \quad (10)$$

$\mathbf{v}(\mathbf{x})$ vanishes and $\mathbf{w}(\mathbf{x}, t)$ remains the only displacement field, the case we consider here.

Moreover, for special choices of the function $f(|\mathbf{r}|)$, Eq. (9) can exhibit analytical solutions, as illustrated in the following sections.

III. ONE-DIMENSIONAL WAVEGUIDE

The one-dimensional version of Eq. (9) is analyzed by our introducing the Gauss-like and the Laplace-like forces [see Eqs. (15) and (18)], for which it simplifies as

$$\rho \frac{\partial^2 w}{\partial t^2} - E \frac{\partial^2 w}{\partial x^2} - g(x) * w(x) = 0, \quad (11)$$

where $g(x) = h_0(x) + f_0(x)$ and $\bar{h} = 0$ and $\bar{f} = 0$ when the force is given by (15) or (18). Since for the aforementioned interaction forces $g(x) = -\partial F(x)/\partial x$, Eq. (11) becomes

$$\rho \frac{\partial^2 w}{\partial t^2} - E \frac{\partial^2 w}{\partial x^2} + F(x) * \varepsilon_x = 0, \quad (12)$$

where ε_x is the strain along the axis, a form consistent with the Eringen formulation for nonlocal elasticity in one dimension [20].

Assuming

$$w(x, t) = \iint_{-\infty}^{+\infty} W(k, \omega) e^{i(kx - \omega t)} dk d\omega, \quad (13)$$

or taking the Fourier transform $\mathcal{F}\{\cdot\}$ of Eq. (11) with respect to x and t , we obtain the dispersion relationship

$$\rho \omega^2 - Ek^2 + G(k) = 0, \quad (14)$$

where $G(k) = \mathcal{F}\{g(x)\}$. Gauss-like and Laplace-like forces reveal some general properties of long-range interaction. These forces present three advantages: (i) they guarantee the action-reaction principle holds, (ii) they vanish for large x , a property typical of some long-range forces encountered in physics, and (iii) they admit an analytical known Fourier transform $G(k)$.

A. Gauss-like interaction

The Gauss-like form is

$$f(r) = \mu e^{-(r/\beta)^2}, \quad (15)$$

where μ controls the intensity of the force and β (positive) is the interaction length. The sign of μ follows the convention stipulated in Sec. II: μ can be positive or negative, representing attractive or repulsive actions, respectively. Moreover, $F(r) = -F(-r)$ and $\lim_{r \rightarrow \infty} F(r) = 0$. Combining Eqs. (15) and (11), we obtain

$$\begin{aligned} \rho \frac{\partial^2 w}{\partial t^2} - E \frac{\partial^2 w}{\partial x^2} - \mu \int_{-\infty}^{+\infty} \left(1 - \frac{2}{\beta^2} \xi^2 \right) \\ \times e^{-(r/\beta)^2} w(x - \xi) d\xi = 0. \end{aligned} \quad (16)$$

For the Gauss-like force, $G(k) = (\mu\beta^3/2\sqrt{2})k^2 e^{-\beta^2 k^2/4}$ and

$$\Omega = \pm K \sqrt{1 - \chi e^{-K^2/4}}, \quad (17)$$

is the dispersion relation associated with Eq. (16), where $\Omega = \sqrt{\rho/E} \beta \omega$, $K = \beta k$, and $\chi = \mu\beta^3/2\sqrt{2}E$ are non-dimensional parameters.

χ is a scale factor that relates the intensity of the long-range interaction in terms of its elastic modulus $E^* = \mu\beta^3/2\sqrt{2}$ (positive or negative) and the elastic modulus E .

As for μ , the sign of χ controls the attraction ($\chi > 0$) or repulsion ($\chi < 0$) characteristic of the force.

Equation (17) can produce, for some wavenumber and χ ranges, imaginary values. This implies the waveguide becomes unstable with unbounded wave amplitudes. This happens for long-range forces of negative equivalent stiffness larger than the classical elastic value.

B. Laplace-like interaction

In this case, f is based on the *Laplace distribution*:

$$f(r) = \mu e^{-|r|/\beta}, \quad (18)$$

with $F(r) = -F(-r)$ and $\lim_{r \rightarrow \infty} F(r) = 0$.

For $G(k) = 2\sqrt{2/\pi}\beta^3 k^2 \mu / (1 + \beta^2 k^2)^2$, the associated dispersion relationship is

$$\Omega = \pm K \sqrt{1 - \frac{8\chi}{\sqrt{\pi}(K^2 + 1)^2}}. \quad (19)$$

C. Notes on the linear approximation

The linear approximation, discussed in Sec. II, implies Eq. (9), and consequently Eq. (11), is valid under the assumption $|\varepsilon| \ll |x - \xi|$. Since $|\varepsilon|/|x - \xi| = |w(x, t) - w(\xi, t)|/|x - \xi| \ll 1$, the strain is small, at least of order 10^{-1} . A wave perturbation travels in the system as $w(x, t) = w_0 e^{j(kx - \omega t)}$. The strain is $\partial w / \partial x = jk w_0 e^{j(kx - \omega t)}$ and the linearization is valid if $|\partial w / \partial x| \ll 1$; hence $|w_0 k| \ll 1$. In terms of the nondimensional wavenumber $K = \beta k$, the condition $|\varepsilon| \ll |x - \xi|$ can be expressed as $|w_0 K / \beta| \ll 1$ and $K \ll \beta / w_0$.

This shows that once the regime for K has been selected (as in the following sections), the amplitude of vibration must be compared with the characteristic interaction length β to guarantee linearization conditions hold.

In the following sections, it appears that for $K \rightarrow \infty$ the propagation characteristic collapses to the standard D'Alembert equation. Therefore, the most-typical and most-interesting aspects of our investigation (wave-stopping and hypersonic velocity) emerge at K of order approximately 1; that is, the studied effects fall in the linearization approximation when the vibration amplitude is much smaller than the characteristic long-range interaction length β : $w_0 \ll \beta$.

IV. WAVE SPEED

The propagation behavior is discussed in terms of χ , which only affects the dispersion equations (17) and (19). From them, with the speed of sound $c = \sqrt{E/\rho}$, analytical forms follow for the group and phase velocity $C_g = (1/c)(\partial\omega/\partial k) = d\Omega/dK$ and $C_\phi = (1/c)(\omega/k) = \Omega/K$, respectively, as well as for the eigenstate density $dN/d\Omega \propto 1/C_g$.

Three ranges for χ are discussed: (i) $\chi \ll -1$, (ii) $-1 < \chi < 1$, and (iii) $\chi \gg 1$.

A. Gauss-like model

1. Negative group velocity and wave-stopping, $\chi \ll -1$

The dispersion curves for $\chi \ll -1$ are presented in Fig. 2, which shows both minimum and maximum points

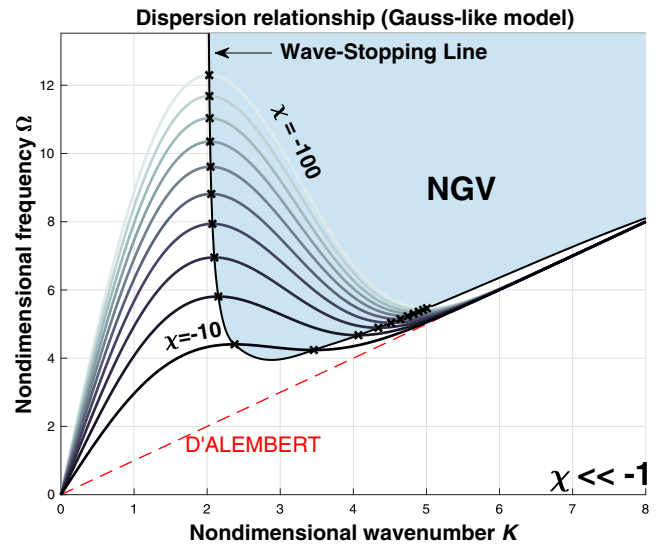


FIG. 2. Dispersion curves for the Gauss-like model for different values of χ .

for each χ . Wave-stopping phenomena appear since at those points the group velocity C_g vanishes (Fig. 3). Moreover, the part of the curves in Fig. 2 with a positive slope is related to a conventional dynamic behavior, while the negative-slope side leads to a negative group velocity.

In Fig. 3, the group velocity is plotted versus the wavenumber. We observe (i) the existence of wavenumber pairs for which the group velocity vanishes, producing wave-stopping, (ii) the presence of a bandwidth of negative values of the group velocity, and (iii) larger wavenumber bandwidth for larger values of $|\chi|$.

As shown in Fig. 4, the phase velocity at low frequencies assumes values considerably higher than those with

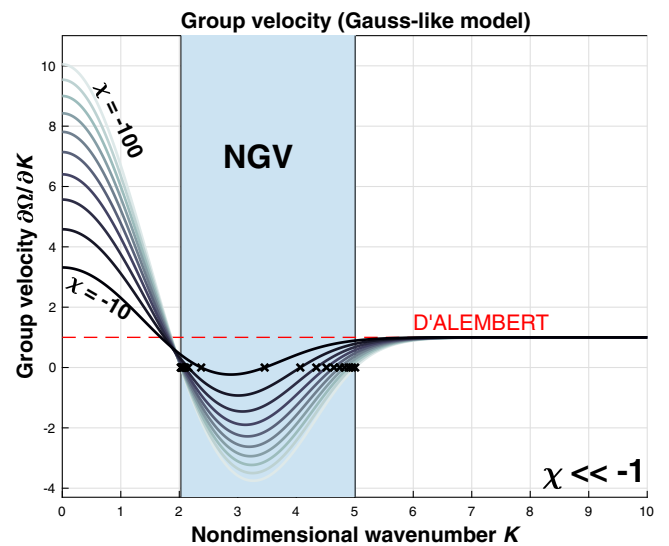


FIG. 3. Group velocity for the Gauss-like model for different values of χ .

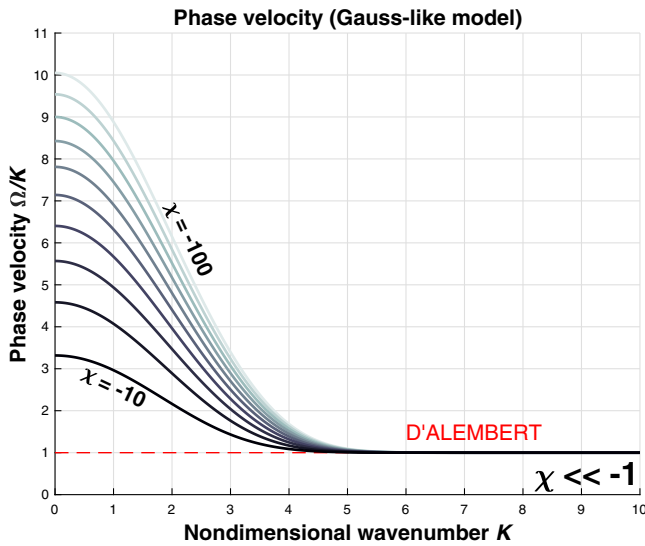


FIG. 4. Phase velocity for the Gauss-like model for different values of χ .

a conventional waveguide, characterized by first-neighbor interactions, and decreases with increasing frequency.

Figure 5 shows the eigenstate density, which exhibits two peaks. These points correspond to the vanishing group velocity.

The singularities in the eigenstate density produce an energy-storage effect in the waveguide, preventing propagation and yielding the inception of wave-stopping.

2. Eigenstate migration, $-1 < \chi < 1$

Wave-dispersion phenomena are analyzed in the range of χ between -1 and 1 characterized by long-range weak

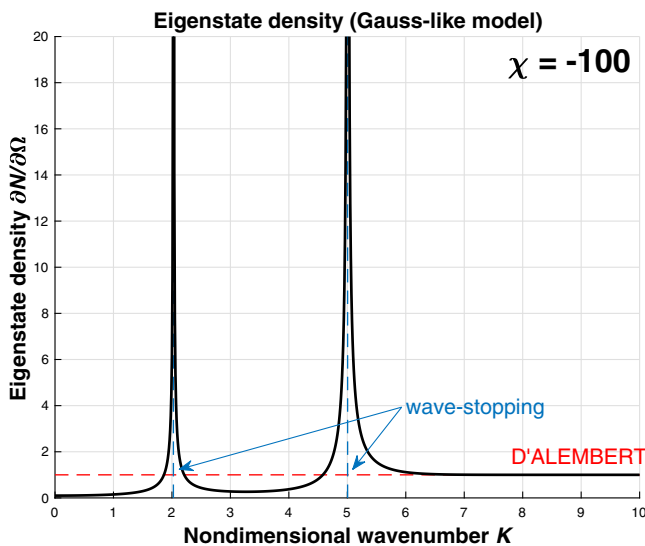


FIG. 5. Eigenstate density for the Gauss-like model for $\chi = -100$.

forces suggesting a behavior close to that of the classical D'Alembert waveguide. Figures 6(a)–6(c) show the trend of the dispersion relationship, the group velocity, and the eigenstate density, respectively. Wave-stopping effects do not occur, and the group velocity is always positive.

However, the eigenstate density, reported in Fig. 6(c), shows a *mode-migration* effect.

For any given χ in Fig. 6(c), two branches of the curve are identified: the one on the right and the one on the left with respect to the intersection with the D'Alembert curve that is at the *folding wavenumber* K_0 . For example, for $0 < \chi < 1$ [Fig. 6(d)], the left branch shows a higher eigenstate density with respect to the D'Alembert case, while the right branch shows a lower eigenstate density. Direct inspection of the analytical expressions for the eigenstate density shows that

$$\int_0^{K_0} \left(\frac{dN}{d\Omega} - 1 \right) d\Omega = \int_{K_0}^{+\infty} \left(1 - \frac{dN}{d\Omega} \right) d\Omega, \quad (20)$$

where $(dN/d\Omega)(K_0) = 1$. This implies that the number of eigenstates gained by the long-range waveguide in the region $K \in [0, K_0]$ equals the number of eigenstates lost in the bandwidth $K \in [K_0, +\infty)$. This means an eigenstate packet migrates from high to low frequency, folding at about K_0 . Analogous considerations hold for $-1 < \chi < 0$.

For all the χ values [see Fig. 6(c)], the characteristic value of K_0 is about 1.4.

The region characterized by a richer eigenstate density tends to trap the energy, slowing its transport and lowering the group velocity [see Figs. 6(b) and 6(c)].

3. Hypersonic group velocity and instability, $\chi \gg 1$

For $\chi \gg 1$, the analysis of propagation reveals the presence of an unstable region: in it, no propagation occurs and wave amplitudes become unbounded (see Fig. 7). In the propagation region, the curves start with a very high slope and the corresponding group velocity ideally becomes infinite; hence, hypersonic (superluminal) group waves are formed.

The group velocity passes from hypersonic (superluminal) propagation to the standard D'Alembert propagation within the wavenumber bandwidth $K \in [\sim 3, \sim 6]$.

B. Laplace-like model

The dispersion relationship and phase and group velocities related to the Laplace-like force have a very similar trend with respect to the Gauss-like interaction, and three identical regimes appear. This enforces the conclusion that the scenario outlined in Sec. IV A has a general character for long-range interaction for those forces that satisfy the requirements in Sec. II.

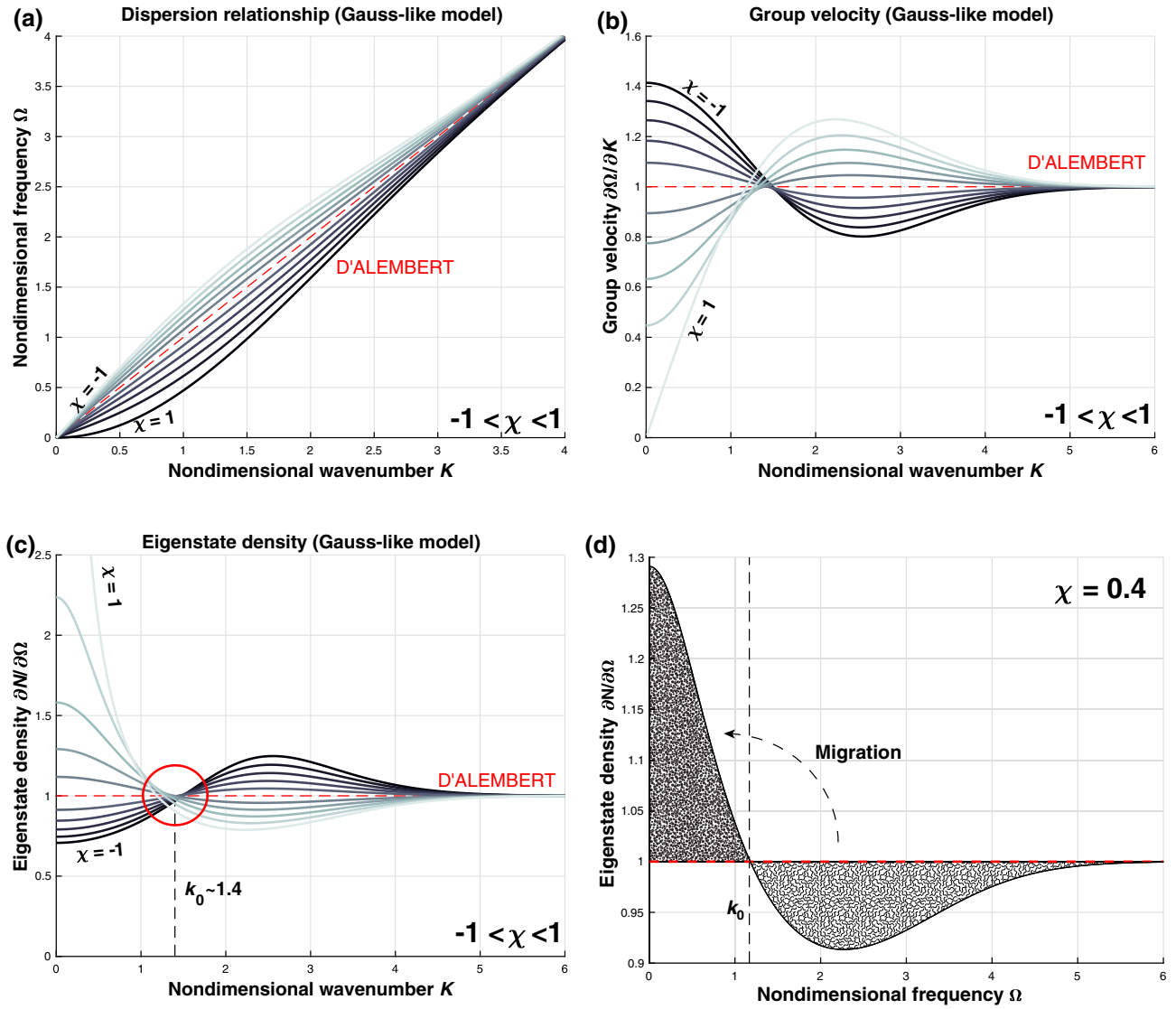


FIG. 6. (a) Dispersion curves, (b) group velocity, and (c), (d) eigenstate density for the Gauss-like model for $\chi \in [-1, 1]$.

V. SPACE-TIME VISUALIZATION

Visualization of the wave propagation in space and time corroborates the previous theoretical findings. Consistent with Eq. (13), waves can be represented by the discrete approximation

$$w(x, t) = \sum_i^N \left\{ W_i^{(1)} \sin[k_i x - \omega(k_i) t] + W_i^{(2)} \cos[k_i x - \omega(k_i) t] \right\}, \quad (21)$$

where $W_i^{(1)}$ and $W_i^{(2)}$ are coefficients depending on the initial conditions, and $\omega(k_i)$ is specified by the dispersion relationships (17) and (19).

Two different graphic representations of the wave pattern are used, both derived from the surface $w(x, t)$ (see Fig. 8).

In Figs. 10, 12, and 14, sections at different times of this surface are shown. The red dots represent the phase velocity and the green squares represent the group velocity. Dotted lines show these points moving in space and time. Figures 11, 13, and 15 show the surface color plot of w over the x, t plane. This permits us to simultaneously identify the wave characteristic lines on x, t , whose inclination remains with the phase propagation, and the envelope peak regions by shaded bands, with inclination proportional to the group velocity.

A. Positive and negative group velocity, wave-stopping effects, $\chi \ll -1$

In Fig. 10, the waveguide response is shown for $\chi = -100$. On the left, a wave-train packet is plotted, with a frequency bandwidth Ω of around ≈ 10 and wavenumber k of about 1.4 (selected along the small arch of the dispersion

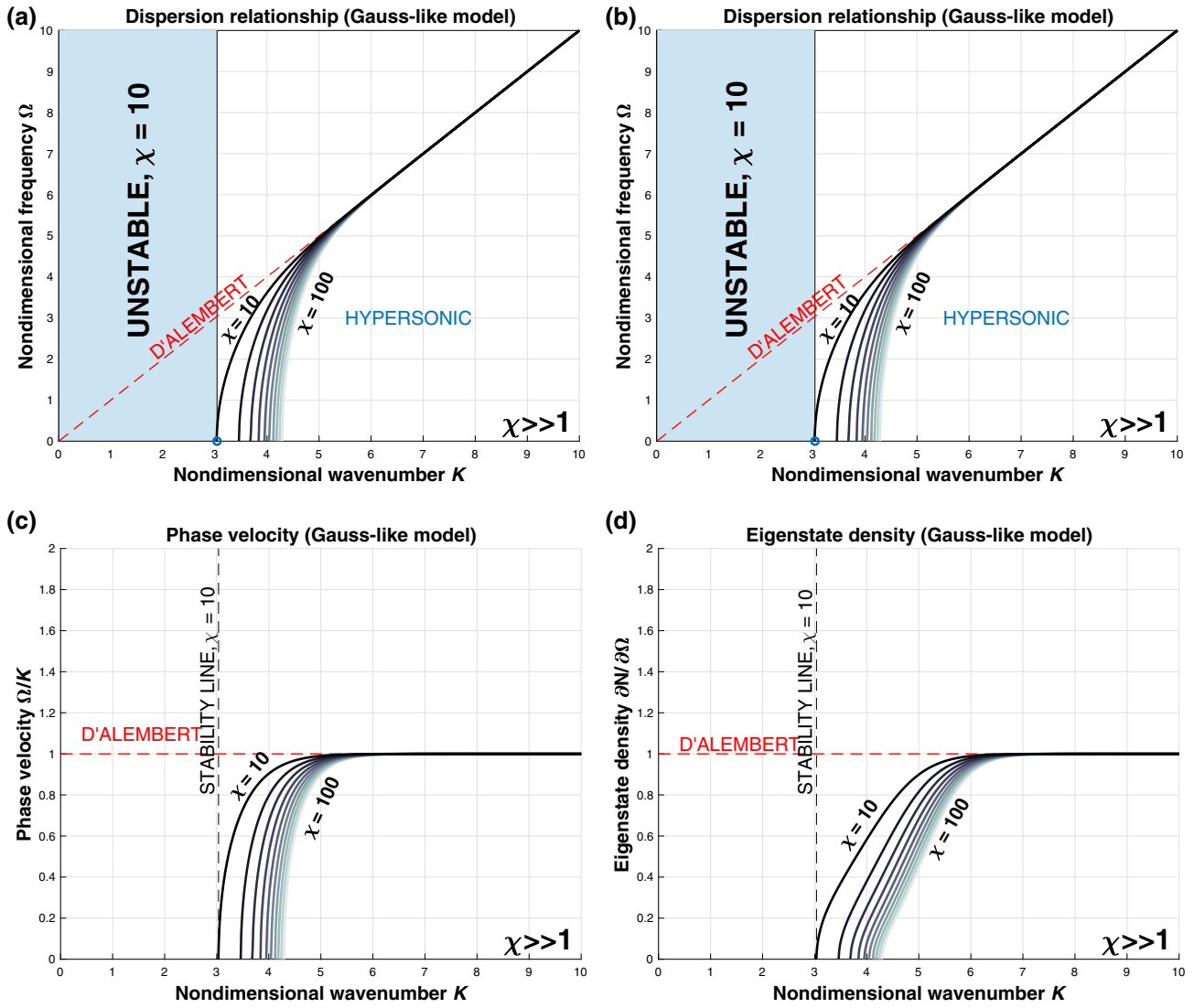


FIG. 7. (a) Dispersion curves, (b) group velocity, (c) phase velocity, and (d) eigenstate density for the Gauss-like model for different values of χ .

curve about A in Fig. 9; i.e., in the positive-group-velocity range). Positive group velocity is observed with a value that is consistent with the findings in Fig. 3. On the right, another wave train is considered with the same frequency bandwidth, but with wavenumbers taken on NGV branch, along a small arch about point B . Figure 10 illustrates the negative-group-velocity effect. The phase wave speed has different values with respect to the group velocity, and they are consistent with those predicted in Fig. 4.

Figure 11 plots the same effect, but following a different representation. Negative slope of shaded bands corresponds to negative group velocity. Phase-speed characteristic lines have different (positive) slopes, again consistent with values shown in Fig. 4.

In Figs. 12 and 13, a wave-train packet is generated with frequencies Ω of about 12 and wavenumber $K = 2$ on a small arch about point C . The left side of Figs. 12 and 13 shows standard waves, and in comparison with the right side, reveals that the long-range effect produces a wave envelope that does not propagate, providing a wave-stopping phenomenon.

B. Hypersonic effect, $\chi \gg 1$

Figure 14 (right) shows the hypersonic (superluminal) propagation of the envelope, compared with the D'Alembert case (left), in which the crest remains substantially close to the centerline. On the right, it also appears that the phase velocity in the long-range case is substantially vanishing according to Fig. 7(c).

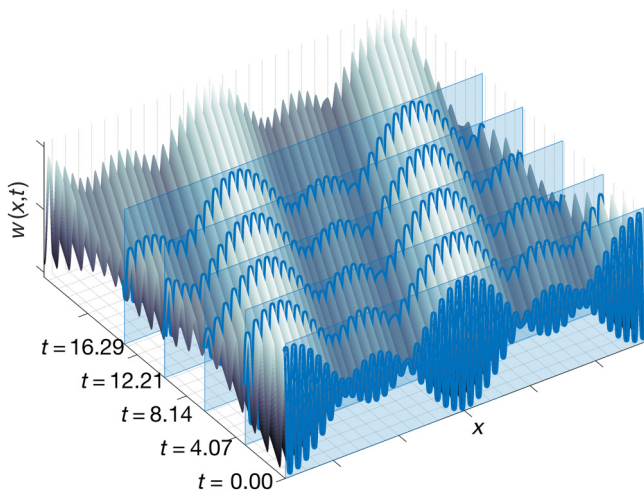


FIG. 8. Three-dimensional surface plot of the displacement.

Figure 15 shows shaded bands with high slope and a striped texture that almost horizontal for phase speed. According to Fig. 7(c), Fig. 15 clearly displays the hyper-sonic (superluminal) effect.

VI. NONLOCAL RETARDED ACTIONS

Since the group velocity can reach, in the range $\chi \gg 1$, even unbounded values [see Fig. 7(c)], it is natural to ask if this effect is implied or related to the instantaneous propagation of the long-range forces. Nonlocal elasticity assumes the force \mathbf{F} acting on the particle at $\mathbf{P}(\mathbf{x})$ due to the particle at $\mathbf{Q}(\xi)$ is transmitted without any delay.

Of course, in many cases, this can be a reasonable approximation when the forces are delayed by negligible

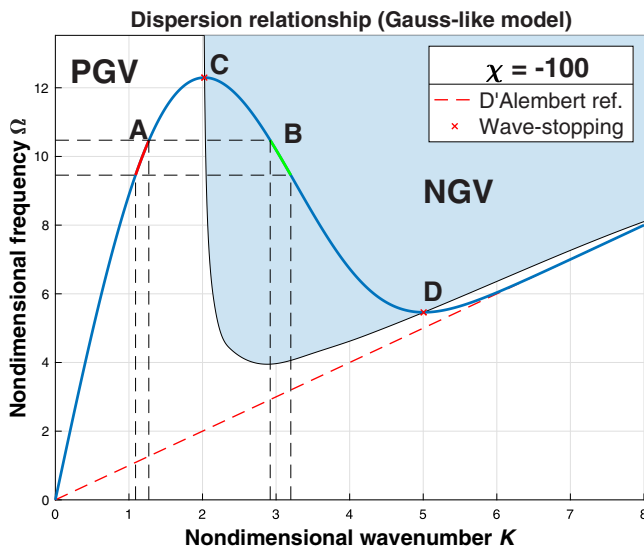


FIG. 9. Selection of four arches (A, B, C, D) of the dispersion curve to generate the wave trains shown in Figs. 10–13. PGV, positive group velocity.

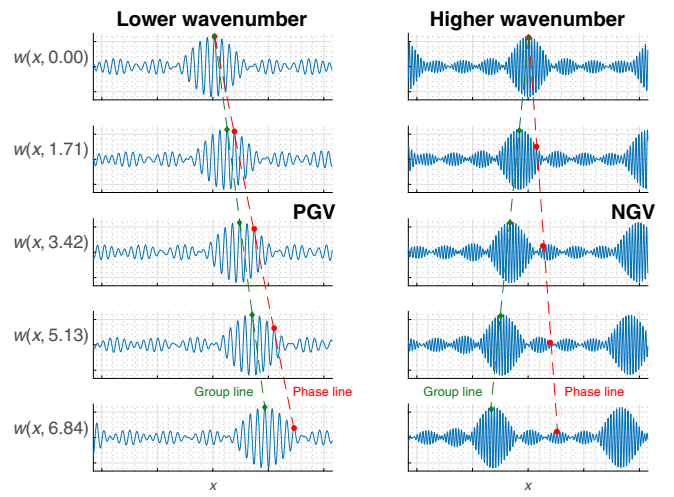


FIG. 10. Positive group velocity (PGV; left) and negative group velocity (right).

time with respect to the characteristic period of oscillation of the particles.

However, simple considerations can reveal the effect of a finite speed v_f of interaction propagation between distant particles, implying the delay $\tau = (x - \xi)/v_f$ of the perturbation at $\mathbf{Q}(\xi)$ to reach $\mathbf{P}(\mathbf{x})$. This transforms Eq. (11) into a delayed integral-differential equation:

$$\rho \frac{\partial^2 w(x, t)}{\partial t^2} - E \frac{\partial^2 w(x, t)}{\partial x^2} - g(x) * w(x, t - \tau) = 0. \quad (22)$$

After some mathematics, the Fourier transform of this equation provides

$$\left[\rho \omega^2 - Ek^2 + G \left(k + \frac{\omega}{v_f} \right) \right] W(k, \omega) = 0. \quad (23)$$

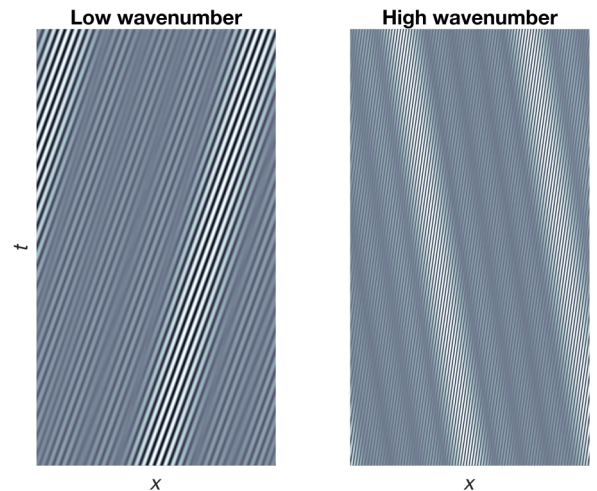


FIG. 11. Surface color plot of $w(x, t)$: positive group velocity (left); negative group velocity (right).

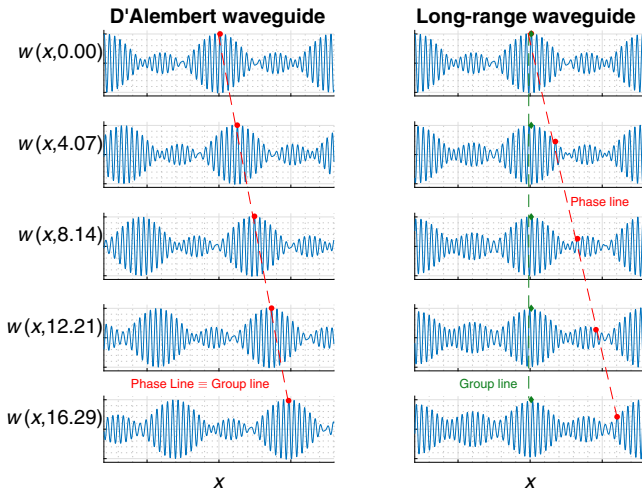


FIG. 12. Wave-stopping effect: D'Alembert waveguide (left); long-range waveguide (right).

If the Gauss-like force is considered, the associated dispersion relationship becomes

$$\Omega^2 - K^2 + \chi \left(K + \frac{\Omega}{V} \right)^2 e^{-\frac{(K+\Omega/V)^2}{4}} = 0, \quad (24)$$

where $V = v_f/c$.

For $V \rightarrow \infty$, Eq. (24) collapses into Eq. (17). For $V \rightarrow 0$, the standard D'Alembert dispersion is obtained.

From Eq. (24), it is deduced that C_g and C_ϕ can be both higher than V , and that C_g can be negative even for $\chi \gg 1$. In particular, for $V = 1$ (i.e., when the speed of the disturbance is comparable with the speed of sound $v_f = c$), the map in Fig. 16 is obtained. With regard the leap line

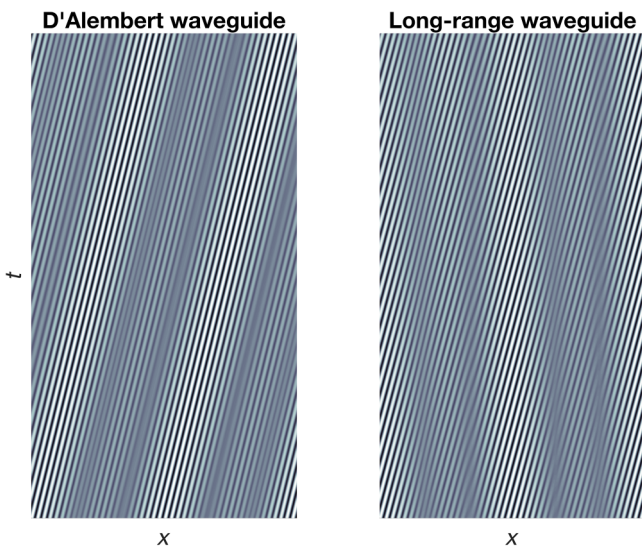


FIG. 13. Surface color plot of $w(x,t)$. Left: D'Alembert waveguide, Right: Long-range waveguide.

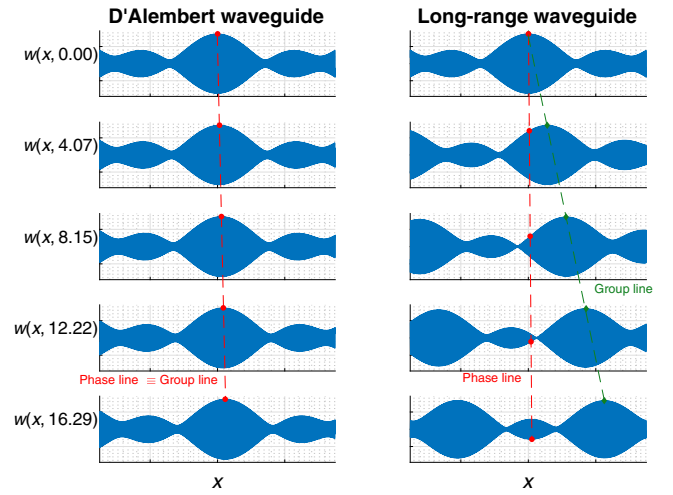


FIG. 14. Hypersonic (superluminal) effect: D'Alembert waveguide (left); long-range waveguide (right).

IASA'I', if we follow it from the point I (asymptotically converging over the line $\chi = 0$) to A , it identifies all the points for which $C_g \rightarrow +\infty$. From A to S , C_g has its maximum, which, however, is finite. From A' to I' , the line identifies all the points for which $C_g = 0$. From A' to S , C_g has its minimum (positive), and there is no chance of wave-stopping.

VII. NOTES ON THE EFFECTS OF DISSIPATION

Historically, the discussion of superluminal effects first appeared in a seminal work of Brillouin [42] in the context of wave propagation in dissipative media, showing the appearance of group velocity that can exceed the speed of light. The previous analysis shows conversely how a

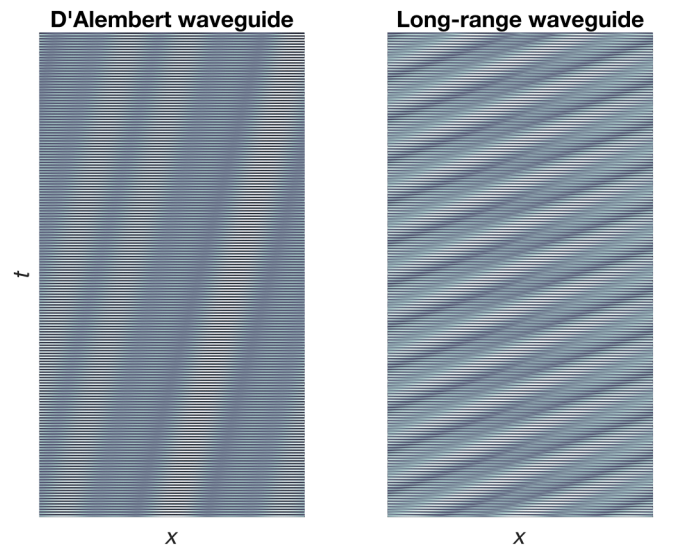


FIG. 15. Surface color plot of $w(x,t)$: D'Alembert waveguide (left); long-range waveguide (right).

loss-free elastic material but with long-range interaction can exhibit similar superluminal effects. It is interesting to explore the combined effects of dissipation and nonlocality, completing Eq. (11) with a viscous term,

$$\rho \frac{\partial^2 w}{\partial t^2} + \gamma \frac{\partial w}{\partial t} - E \frac{\partial^2 w}{\partial x^2} - g(x) * w(x) = 0, \quad (25)$$

which leads to the nondimensional dispersion relationship

$$\Omega = -j \frac{\Gamma}{2} \pm \sqrt{Q^2 - \left(\frac{\Gamma}{2}\right)^2}, \quad (26)$$

where $\Gamma = \gamma\beta/\sqrt{\rho E}$, $Q^2 = K^2[1 - \chi\phi(K)]$ and $\phi(K) = e^{-K^2/4}$, $\phi(K) = 8/(K^2 + 1)^2$ for the Gaussian and Laplace cases, respectively. The group velocity, in this case, becomes complex:

$$\begin{aligned} c_g &= \frac{\partial \Omega}{\partial K} = \pm \frac{1}{\sqrt{1 - (\Gamma/2Q)^2}} \frac{\partial Q}{\partial K} \\ &= \pm \frac{1}{\sqrt{1 - (\Gamma/2Q)^2}} c_{g\Gamma=0}, \end{aligned} \quad (27)$$

in which the long-range and dissipation effects appear in a factorized form.

Let us analyze the two extreme cases. In the absence of dissipation, $\Gamma = 0$, and then $c_g = c_{g\Gamma=0}$, which is the group velocity discussed in the previous sections. In the absence of long-range interactions, $Q = K$, and then $\partial Q/\partial K = 1$ and the group velocity becomes $c_g = \pm 1/\sqrt{1 - (\Gamma/2Q)^2}$, which can be discussed in terms of Γ to assert superluminal effects (i.e., $c_g > 1$) as in Ref. [42]. This happens for $\sqrt{1 - (\Gamma/2Q)^2} < 1$ and $\sqrt{1 - (\Gamma/2Q)^2}$ real. When both effects are simultaneously present, the real part of c_g can be larger or smaller than 1 depending on the choices of Γ and χ .

We conclude that in the presence of both long-range interaction and dissipation, superluminality can appear. Moreover, the two effects can cooperate or compete in producing superluminal effects, depending on the frequency range considered and the intensity of the dissipation and long-range forces. As a final conclusion, dissipation is not a necessary condition to obtain superluminality. This corroborates the observations of Wang *et al.* [44], who concluded that ‘‘superluminal group velocity is possible. . . with no appreciable absorption or amplification.’’

VIII. PROPAGATION MAP AND CONCLUSIONS

The present investigation defines how long-range interactions in elastic metamaterials can produce a variety of effects in wave propagation.

A complete theoretical analysis is presented, based on two families of nonlocal interactions: Gauss-like and Laplace-like interactions. They have the merit to rapidly decay with distance, to fulfill the action-reaction principle requirement, and to be available for closed-form investigation of their dispersion relationships. Their general nature corroborates the idea that the properties deduced for them are representative of a general scenario expected for a large class of elastic metamaterials (and possibly for a class of long-range interactions in a lattice or in charged gases).

The study is conducted by our embedding the long-range forces of exponential type $f(r) = \mu e^{-(r/\beta)^2}$ in a conventional elastic waveguide and discussing the effect they produce, on the basis of a single dimensionless parameter $\chi = E^*/E$. It takes into account the ratio of the long-range elastic modulus $E^* = \mu\beta^3/2\sqrt{2}$ and of Young’s modulus E . E^* can be either positive or negative depending on the attractive or repulsive nature of the interaction force.

Two opposite scenarios emerge for different values of E^* : large and negative E^* leads to wave-stopping and negative group velocity; large and positive E^* produces hypersonic (superluminal) effects at the boundary with an unstable region. When $|E^*|$ is close to E , none of the previous effects are observed, but an eigenstate migration appears that moves the system modes from higher to lower frequency or vice versa, identifying a characteristic folding wavenumber. A propagation map is depicted in Fig. 17 (with equal-frequency contours), in which all the scenarios investigated in this paper for $V = +\infty$ are reported for the Gauss-like case. In particular, we can identify the NGV region, bounded by the wave-stopping curve, and the unstable region, delimited by the hypersonic (superluminal) curve separating from the instability region (at $\Omega = 0$).

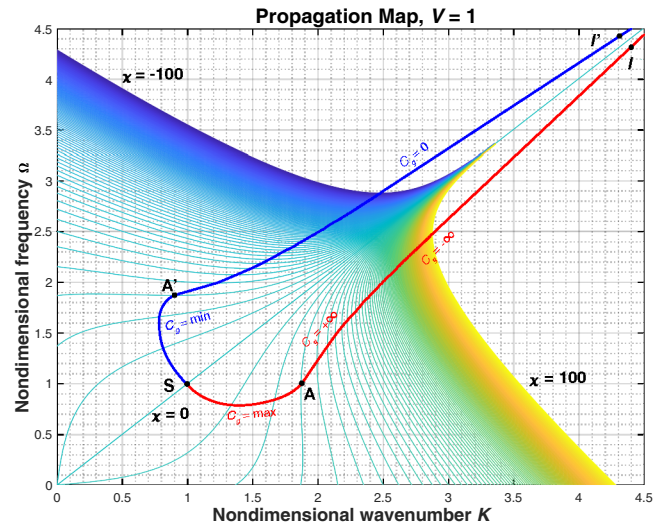


FIG. 16. Group velocity and superluminal effect for a retarded signal with $V = 1$.

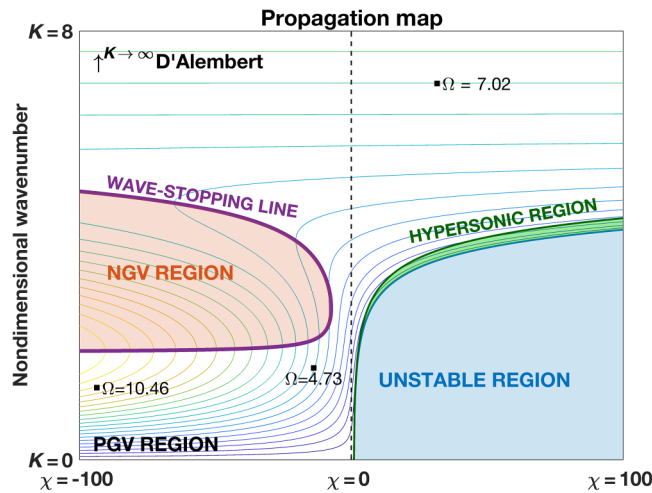


FIG. 17. Propagation map for instant long-range interaction. PGV, positive group velocity.

Finally, the combined effect of retarded and long-range actions is investigated. It is shown that even if a limit speed v_f exists for the interaction signal, the group and phase velocity can still be higher than v_f , a possibility discussed in Ref. [42].

Finally, the effect of dissipation is investigated, and it is demonstrated to be not crucial to obtain superluminality. Long-range elastic interaction produces superluminality even in the absence of dissipative effects.

Because of the properties of the Gauss-like force, essentially of type decaying with the distance, we can conjecture these maps have a universal character in describing the expected scenarios for long-range interactions in metamaterials. Their use could represent a reference for designing new metamaterials with desired specific properties.

The theoretical background presented has wider potential uses. The long-distance interaction is a recurring challenge in physics. Statistical mechanics of complex systems is classically based on Boltzmann theory and the collision integral represents typical “short-range” interactions.

The Vlasov theory considers long-range interaction for the evaluation of the probability density of a system of charged particles as electrons or plasma ions. Long-range thermodynamics [45] produces unusual effects as negative specific heat, anomalous diffusion, ergodicity breaking, and new regimes in cold gases.

The model introduced in this paper provides, in this respect, an interpretation of deterministic effects that can be expected for long-range retarded interactions.

Beyond physics, the population dynamics has a very interesting aspect that relates to the interaction range. Recent studies in crowd dynamics [46] propose models of social forces including repulsive or attractive actions, and these models can be used to predict catastrophic scenarios [47]. Traffic modeling is one of the possibilities these models offer [48].

The mathematical model of waves generated in a population of particles, as in the present investigation, can be interpreted as the collective behavior of a population of individuals, the mutual interactions of which produce faster or slower social effects. The retarded action shows the effects of communication delay between a pair of individuals that affects the global response of the community.

- [1] Vincent Laude and Maria E. Korotyaeva, Stochastic band structure for waves propagating in periodic media or along waveguides, arXiv preprint arXiv:1801.09914 (2018).
- [2] Andres D. Neira, Gregory A. Wurtz, and Anatoly V. Zayats, Superluminal and stopped light due to mode coupling in confined hyperbolic metamaterial waveguides, *Sci. Rep.* **5**, 17678 (2015).
- [3] D. E. Chang, Amir H. Safavi-Naeini, Mohammad Hafezi, and Oskar Painter, Slowing and stopping light using an optomechanical crystal array, *New J. Phys.* **13**, 023003 (2011).
- [4] Mehmet Fatih Yanik and Shanhui Fan, Stopping Light all Optically, *Phys. Rev. Lett.* **92**, 083901 (2004).
- [5] Kosmas L. Tsakmakidis, Tim W. Pickering, Joachim M. Hamm, A. Freddie Page, and Ortwin Hess, Completely stopped and dispersionless light in plasmonic waveguides, *Physical Rev. Lett.* **112**, 167401 (2014).
- [6] Dexin Ye, Yannick Salamin, Jiangtao Huangfu, Shan Qiao, Guoan Zheng, and Lixin Ran, Observation of wave packet distortion during a negative-group-velocity transmission, *Sci. Rep.* **5**, 8100 (2015).
- [7] David Maximilian Storch, Mauritz Van den Worm, and Michael Kastner, Interplay of soundcone and supersonic propagation in lattice models with power law interactions, *New J. Phys.* **17**, 063021 (2015).
- [8] Jingyuan Qu, Alexander Gerber, Frederik Mayer, Muamer Kadic, and Martin Wegener, Experiments on Metamaterials with Negative Effective Static Compressibility, *Phys. Rev. X* **7**, 041060 (2017).
- [9] Nicolas Brunner, Valerio Scarani, Mark Wegmüller, Matthieu Légré, and Nicolas Gisin, Direct Measurement of Superluminal Group Velocity and Signal Velocity in an Optical Fiber, *Phys. Rev. Lett.* **93**, 203902 (2004).
- [10] W. M. Robertson, J. Pappafotis, P. Flannigan, J. Cathey, B. Cathey, and C. Klaus, Sound beyond the speed of light: Measurement of negative group velocity in an acoustic loop filter, *Appl. Phys. Lett.* **90**, 014102 (2007).
- [11] D. Mugnai, A. Ranfagni, and R. Ruggeri, Observation of Superluminal Behaviors in Wave Propagation, *Phys. Rev. Lett.* **84**, 4830 (2000).
- [12] Michael D. Stenner, Daniel J. Gauthier, and Mark A. Neifeld, The speed of information in a ‘fast-light’ optical medium, *Nature* **425**, 695 (2003).
- [13] B. Shokri, S. KhAlavi, and A. A. Rukhadze, Surface waves on a piezo-plasma-like medium, *Phys. Scr.* **73**, 23 (2005).
- [14] Carmel Rotschild, Barak Alfassi, Oren Cohen, and Mordechai Segev, Long-range interactions between optical solitons, *Nat. Phys.* **2**, 769 (2006).

- [15] Boris M. Smirnov, *Fundamentals of Ionized Gases: Basic Topics in Plasma Physics* (John Wiley & Sons, Weinheim, Germany, 2012).
- [16] Victor A. Eremeyev, Leonid P. Lebedev, and Holm Altenbach, *Foundations of Micropolar Mechanics* (Springer Science & Business Media, Heidelberg, New York, Dordrecht, London, 2012).
- [17] Antonio Carcaterra, F. Dell’Isola, R. Esposito, and M. Pulvirenti, Macroscopic description of microscopically strongly inhomogeneous systems: A mathematical basis for the synthesis of higher gradients metamaterials, *Arch. Ration. Mech. Anal.* **218**, 1239 (2015).
- [18] A. Cemal Eringen, Plane waves in nonlocal micropolar elasticity, *Int. J. Eng. Sci.* **22**, 1113 (1984).
- [19] A. Cemal Eringen, Linear theory of micropolar elasticity, *J. Math. Mech.* **15**, 909 (1966).
- [20] A. Cemal Eringen, Linear theory of nonlocal elasticity and dispersion of plane waves, *Int. J. Eng. Sci.* **10**, 425 (1972).
- [21] Noël Challamel, Lalaonirina Rakotomanana, and Loïc Le Marrec, A dispersive wave equation using nonlocal elasticity, *CR Mécanique* **337**, 591 (2009).
- [22] Z. Rueger and R. S. Lakes, Strong Cosserat Elasticity in a Transversely Isotropic Polymer Lattice, *Phys. Rev. Lett.* **120**, 065501 (2018).
- [23] Tobias Frenzel, Muamer Kadic, and Martin Wegener, Three-dimensional mechanical metamaterials with a twist, *Science* **358**, 1072 (2017).
- [24] Daniel Torrent, Yan Pennec, and Bahram Djafari-Rouhani, Resonant and nonlocal properties of phononic metasolids, *Phys. Rev. B* **92**, 174110 (2015).
- [25] Leon Brillouin, *Wave Propagation in Periodic Structures: Electric Filters and Crystal Lattices* (Courier Corporation, New York, 2003).
- [26] Walter A. Harrison, *ibid.* 136, a1107 (1964), *Phys. Rev.* **136**, A1107 (1964).
- [27] Dionisio Del Vescovo and Ivan Giorgio, Dynamic problems for metamaterials: Review of existing models and ideas for further research, *Int. J. Eng. Sci.* **80**, 153 (2014).
- [28] Vasily E. Tarasov and George M. Zaslavsky, Fractional dynamics of coupled oscillators with long-range interaction, *Chaos* **16**, 023110 (2006).
- [29] Vasily E. Tarasov, Continuous limit of discrete systems with long-range interaction, *J. Phys. A: Math. Gen.* **39**, 14895 (2006).
- [30] Angela Madeo, Gabriele Barbagallo, Marco Valerio d’Agostino, Luca Placidi, and Patrizio Neff, in *Proc. R. Soc. A* (The Royal Society, London, 2016), Vol. 472, p. 20160169.
- [31] Dexin Ye, Guoan Zheng, Jingyu Wang, Zhiyu Wang, Shan Qiao, Jiangtao Huangfu, and Lixin Ran, Negative group velocity in the absence of absorption resonance, *Sci. Rep.* **3**, 1628 (2013).
- [32] Mario Di Paola, Giuseppe Failla, Antonina Pirrotta, Alba Sofi, and Massimiliano Zingales, The mechanically based non-local elasticity: An overview of main results and future challenges, *Phil. Trans. R. Soc. A* **371**, 20120433 (2013).
- [33] Richard Phillips Feynman and F. L. Vernon, Jr., The theory of a general quantum system interacting with a linear dissipative system, *Ann. Phys.* **281**, 547 (2000).
- [34] Francisco Jauffred, Roberto Onofrio, and Bala Sundaram, Universal and anomalous behavior in the thermalization of strongly interacting harmonically trapped gas mixtures, *J. Phys. B: Atom. Mol. Opt. Phys.* **50**, 135005 (2017).
- [35] Amir O. Caldeira and Anthony J. Leggett, Path integral approach to quantum Brownian motion, *Physica A* **121**, 587 (1983).
- [36] Antonio Carcaterra and A. Akay, Dissipation in a finite-size bath, *Phys. Rev. E* **84**, 011121 (2011).
- [37] Antonio Carcaterra and A. Akay, Fluctuation-dissipation and energy properties of a finite bath, *Phys. Rev. E* **93**, 032142 (2016).
- [38] A. D. Pierce, Resonant-frequency-distribution of internal mass inferred from mechanical impedance matrices, with application to fuzzy structure theory, *J. Vib. Acoust.* **119**, 324 (1997).
- [39] A. A. Vlasov, On high-frequency properties of electron gas, *J. Exp. Theor. Phys.* **8**, 291 (1938).
- [40] Varun D. Vaidya, Yudan Guo, Ronen M. Kroeze, Kyle E. Ballantine, Alicia J. Kollár, Jonathan Keeling, and Benjamin L. Lev, Tunable-Range, Photon-Mediated Atomic Interactions in Multimode Cavity QED, *Phys. Rev. X* **8**, 011002 (2018).
- [41] Shruti Puri, Christian Kraglund Andersen, Arne L. Grimsmo, and Alexandre Blais, Quantum annealing with a network of all-to-all connected, two-photon driven Kerr nonlinear oscillators, arXiv preprint arXiv:1609.07117 (2016).
- [42] Léon Brillouin, *Wave Propagation and Group Velocity*, Vol. 8 (Academic Press, New York and London, 2013).
- [43] Shaukat Ali Shan and Q. Haque, Low frequency electrostatic nonlinear structures in an inhomogeneous magnetized non-Maxwellian electron–positron–ion plasma, *Phys. Lett. A* **382**, 99 (2018).
- [44] L. J. Wang, A. Kuzmich, and A. Dogariu, Erratum: Gain-assisted superluminal light propagation, *Nature* **406**, 277 (2000).
- [45] Freddy Bouchet, Shamik Gupta, and David Mukamel, Thermodynamics and dynamics of systems with long-range interactions, *Physica A* **389**, 4389 (2010).
- [46] Dirk Helbing, Ansgar Hennecke, Vladimir Shvetsov, and Martin Treiber, Micro-and macro-simulation of freeway traffic, *Math. Comput. Model.* **35**, 517 (2002).
- [47] H. Gayathri, P. M. Aparna, and Ashish Verma, A review of studies on understanding crowd dynamics in the context of crowd safety in mass religious gatherings, *Int. J. Disaster Risk Reduct.* **25**, 82 (2017).
- [48] Dirk Helbing and Peter Molnar, Social force model for pedestrian dynamics, *Phys. Rev. E* **51**, 4282 (1995).